



DØ note 6426-CONF

**Measurement of the Effective Weak Mixing Angle ( $\sin^2 \theta_{\text{eff}}^\ell$ ) in  $p\bar{p} \rightarrow Z/\gamma^* \rightarrow e^+e^-$  events at  $\sqrt{s} = 1.96$  TeV**

The DØ Collaboration  
URL <http://www-d0.fnal.gov>  
(Dated: March 19, 2014)

Preliminary Results for Winter 2014 Conferences

We present a measurement of the weak mixing angle in  $p\bar{p} \rightarrow Z/\gamma^* \rightarrow e^+e^-$  events at a center of mass energy of 1.96 TeV, using  $9.7 \text{ fb}^{-1}$  data collected by the DØ detector at the Fermilab Tevatron. The effective weak mixing angle is extracted from the forward-backward charge asymmetry distribution as a function of the dielectron invariant mass around the  $Z$  pole. In this analysis the event sample is increased by 85% with respect to the expected sample of  $9.7 \text{ fb}^{-1}$  data, primarily by extending the geometric acceptance of electrons, and the systematic uncertainty is reduced by applying a new energy calibration method. The measured value of  $\sin^2 \theta_{\text{eff}}^\ell$ ,  $0.23106 \pm 0.00053$ , is the most precise measurement from light quark interactions and has a precision comparable to the best individual LEP collaboration result and SLD result [1].

## INTRODUCTION

The weak mixing angle  $\sin^2 \theta_W$  is one of the fundamental constants of the standard model (SM). It describes the relative strength of the axial-vector couplings  $g_A^f$  to the vector couplings  $g_V^f$  in the neutral-current interactions of a  $Z$  boson to fermions  $f$  at the Born level as

$$-i \frac{g}{2 \cos \theta_W} \bar{f} \gamma^\mu \left( g_V^f - g_A^f \gamma_5 \right) f Z_\mu \quad (1)$$

with

$$g_V^f = I_3^f - 2Q_f \cdot \sin^2 \theta_W \quad (2)$$

$$g_A^f = I_3^f \quad (3)$$

where  $I_3^f$  and  $Q_f$  are the weak isospin component and the charge of the fermion. At tree level or at all orders of the on-shell renormalization scheme, the parameter can be written in terms of the  $W$  and  $Z$  boson mass as  $\sin^2 \theta_W = 1 - M_W^2/M_Z^2$ . To include higher-order electroweak radiative corrections, fermion flavor-specific effective couplings are defined as

$$\sin^2 \theta_{\text{eff}}^f = \frac{1}{4|Q_f|} \left( 1 - \frac{g_V^f}{g_A^f} \right), \quad (4)$$

and it is customary to quote the charged lepton effective weak mixing angle  $\sin^2 \theta_{\text{eff}}^\ell$ , which can be determined by parity violating observations around the  $Z$  boson mass pole. The two most precise measurements of  $\sin^2 \theta_{\text{eff}}^\ell$ , the charge asymmetry for  $b$  quark production  $A_{FB}^{0,b}$ , where the combined LEP measurement is  $0.23221 \pm 0.00029$ , and the electron-positron left-right polarization asymmetry  $A_l$ , measured by the SLD Collaboration to be  $0.23098 \pm 0.00026$  [1], differ by more than three standard deviations. Therefore, an independent determination of the weak mixing angle is an important precision test of the SM electroweak symmetry breaking mechanism.

At the Tevatron, the mixing angle can be determined in the Drell-Yan process  $q\bar{q} \rightarrow Z/\gamma^* \rightarrow \ell^+\ell^-$ , through a forward-backward charge asymmetry in the emission angle ( $\theta^*$ ) distribution of the negatively charged lepton momentum relative to the incoming quark momentum, defined in the Collins-Soper frame [2]. Events with  $\cos \theta^* > 0$  are classified as forward (F), and those with  $\cos \theta^* < 0$  as backward (B). The forward-backward charge asymmetry,  $A_{FB}$ , is defined by

$$A_{FB} = \frac{N_F - N_B}{N_F + N_B}, \quad (5)$$

where  $N_F$  and  $N_B$  are the numbers of forward and backward events.

$A_{FB}$  can be measured as a function of the invariant mass of the dilepton pair ( $M_{ee}$ ). The presence of both vector and axial-vector couplings of the  $Z$  boson to fermions gives the largest variation of the  $A_{FB}$  value in the vicinity of the  $Z$  pole, providing a sensitive probe of the effective weak mixing angle.

The parameter  $\sin^2 \theta_{\text{eff}}^\ell$  has been measured previously by the CDF collaboration in the  $Z \rightarrow e^+e^-$  [3, 4] and  $Z \rightarrow \mu^+\mu^-$  [5] channels, and the D0 collaboration in the  $Z \rightarrow e^+e^-$  channel [6, 7]. The parameter  $\sin^2 \theta_{\text{eff}}^\ell$  has also been measured at the Large Hadron Collider (LHC) in  $pp$  collisions by the CMS [8] collaboration using an integrated luminosity of  $1.1 \text{ fb}^{-1}$  in  $Z \rightarrow \mu^+\mu^-$  channel.

This note reports a measurement of the effective weak mixing angle from the  $A_{FB}$  distribution using  $9.7 \text{ fb}^{-1}$  of data collected with the D0 detector at the Fermilab Tevatron collider. The largest integrated luminosity previously used by the D0 collaboration to measure  $A_{FB}$  and  $\sin^2 \theta_{\text{eff}}^\ell$  was  $5 \text{ fb}^{-1}$  of data in the di-electron channel [7]. The accuracy of the measured weak mixing angle,  $0.2309 \pm 0.0008$  (stat.)  $\pm 0.0006$  (syst.), was limited by the size of the data sample and the dominant systematic uncertainty, which was the electron energy scale. This analysis with  $9.7 \text{ fb}^{-1}$  features an extended acceptance and a new electron energy calibration method and yields the most precise direct measurement of  $\sin^2 \theta_{\text{eff}}^\ell$  to date from a hadron collider.

## The D0 Detector

The D0 detector [9] comprises a central tracking system, a calorimeter and a muon system. The central tracking system consists of a silicon microstrip tracker (SMT) and a scintillating central fiber tracker (CFT), both located within a 2 T superconducting solenoidal magnet and optimized for tracking and vertexing capabilities at detector pseudorapidities of  $|\eta_{\text{det}}| < 3$  [10]. Outside the solenoid, three liquid argon and uranium calorimeters provide coverage of  $|\eta_{\text{det}}| < 4.2$ : the central calorimeter (CC) up to  $|\eta_{\text{det}}| < 1.1$ , and two endcap calorimeters (EC) in the range  $1.5 < |\eta_{\text{det}}| < 4.2$ . Gaps between the cryostats create an inefficient electron detection region between  $1.1 < |\eta_{\text{det}}| < 1.5$  that is excluded from the analysis.

## SAMPLES and EVENT SELECTION

The data used in this analysis are collected by triggers requiring at least two electromagnetic (EM) clusters reconstructed in the calorimeter. The two EM clusters are further required to be in the CC or EC, with transverse momentum  $p_T > 25$  GeV/ $c$ , and to have shower shapes consistent with that of an electron. For events with both EM candidates in the CC region (CC-CC), each EM object must have a spatially matched track reconstructed in the tracking system; for events with one EM cluster in the CC and the other in the EC region (CC-EC), only the CC candidate is required to have a matched track; while for events with both candidates in the EC calorimeter (EC-EC), at least one EM object must have a matched track. Four types of tracks are defined according to strict reconstruction quality requirements that depend on the different geometric coverage of tracking system components, and all track types must have  $p_T > 10$  GeV/ $c$ . For CC-CC events, the two EM candidates are required to have opposite charges. For CC-EC events, the determination of forward or backward is made according to the charge of the CC EM candidate with a matched track; while for EC-EC events, the charge of the higher quality matched track is used to determine if the event is forward or backward [11].

Events are further required to have a reconstructed dielectron invariant mass in the range  $75 < M_{ee} < 115$  GeV/ $c^2$ . An enlarged sample satisfying  $60 < M_{ee} < 130$  GeV/ $c^2$  is used to understand detector responses and to tune the Monte Carlo (MC) simulation.

To maximize the acceptance, electrons reconstructed near the calorimeter sampling module boundary [9] (phi-mod boundary) of the CC are now included in the data set. The geometric acceptance is further extended from  $|\eta_{\text{det}}| < 1.0$  to  $|\eta_{\text{det}}| < 1.1$  for the CC, and from  $1.5 < |\eta_{\text{det}}| < 2.5$  to  $1.5 < |\eta_{\text{det}}| < 3.2$  for the EC, compared with previous D0 results [7]. The EC-EC events, which were excluded in the previous D0 analysis due to their comparatively worse track reconstruction and energy resolution, are now included. These extensions in  $\eta_{\text{det}}$  and phi-mod acceptance result in a 70% increase in the number of events in the data sample. An additional 15% increase is gained from improvements in the track reconstruction algorithm. The increase from extensions and improvements in the track reconstruction algorithm is above gains from the integrated luminosity. The number of  $Z \rightarrow e^+e^-$  candidate events in the data sample is 560,267 including 248,380 CC-CC events, 240,593 CC-EC events and 71,294 EC-EC events.

The MC Drell-Yan  $Z/\gamma^* \rightarrow e^+e^-$  sample is generated by using the standard D0 simulation software, based on the leading-order PYTHIA generator [12] with the CTEQ6L1 [13] parton distribution functions (PDFs), followed by a GEANT-based simulation [14] of the D0 detector. The PYTHIA MC samples, with events from random beam crossings overlaid, are mainly used to understand the detector's geometric acceptance, and the energy scale and resolution of electrons in the calorimeter.

## ENERGY MODELING

### I. ENERGY CALIBRATION

A new method of electron energy calibration is developed and applied to both the data and MC. This significantly reduces the relevant systematic uncertainty that comes from modeling the response of the calorimeter to electrons energy. The weak mixing angle is extracted from  $A_{FB}$  as a function of the dielectron invariant mass, and depends strongly on the position of the peak value of the invariant mass. Therefore, it is critical to have a precise electron energy modeling and a consistent mass peak value of the dielectron reconstructed mass from different regions of the detector across various Tevatron running conditions. In the previous paper [7], an overall scale factor was applied to the simulation to model the detector response for the energy by electrons. The scale factor was determined by comparing the invariant mass spectrum in the data and the MC, and included a large uncertainty due to the background estimation and detector resolution. In this analysis, a new energy calibration method is introduced to tune the data and the MC separately. The energy calibration is performed by applying luminosity and  $\eta_{\text{det}}$  dependent correction functions to the electron energy. Factors in the correction functions are tuned by requiring the peak of the  $M_{ee}$  distribution to coincide with the  $Z$  boson mass measured by LEP (91.1875 GeV) [1]. After the energy calibration, the deviation of the dielectron invariant mass peak value as a function of instantaneous luminosity and  $\eta_{\text{det}}$  is smaller than 100 MeV in the data and 10 MeV in the MC. Evaluation of the systematic uncertainty associated with the  $Z$ -pole energy scale calibration has not yet been completed. Variations of the functional form of the correction are being investigated, as well as studies of pseudoexperiments based on the  $M_{ee}$  distributions from CC-CC, CC-EC, and EC-EC events. An upper bound on the energy scale uncertainty can be estimated by taking the global energy scale uncertainty from the  $5 \text{ fb}^{-1}$  measurement (0.00022), and scaling it down by the square root of the increase in  $Z$  statistics ( $\sqrt{3.8}$ ), yielding a very conservative uncertainty estimate of 0.00012.

## II. MC ENERGY RESOLUTION

After the electron energy calibration, and additional energy resolution smearing is developed and applied to the MC to achieve the agreement with the data. For electrons in the vicinity of the CC phi-mod boundaries, the resolution smearing is modeled with a Crystal Ball function. For other electrons, the smearing is modeled with a Gaussian function.

## OTHER MC CORRECTIONS

Additional corrections and reweightings are applied to the MC to improve the agreement with data. Scale factors of the electron identification efficiency between the MC and the data are measured using the standard tag-probe method [15] and applied to the MC as functions of  $p_T$  and  $\eta$ . The statistical fluctuation in the measurement of efficiencies is used to estimate the final uncertainty on  $\sin^2 \theta_W$ . The simulation is further corrected for higher-order effects not included in PYTHIA. The MC events are reweighted at the generator level in two dimensions ( $Z$  boson  $p_T$  and rapidity) to match the RESBOS [16] predictions, and additionally the next-to-next-leading order QCD correction has been applied as a function of the  $Z$  boson mass.

The instantaneous luminosity and primary vertex distributions are also reweighted to match those in data. Due to the fact that the  $A_{FB}$  is defined as a ratio of numbers of events, only the electron selection efficiency scale factor will contribute to the final uncertainty.

The charge of the track matched to the EM cluster is used to determine if the EM cluster is an electron or positron and to classify the event as forward or backward accordingly. The charge misidentification rates of different types of tracks are measured in both the data and the MC, and the charge of electrons and positrons reconstructed in the MC is randomly changed to match the charge misidentification probability in the data. The statistical fluctuations in the charge misidentification rate measured from data are included as a systematic uncertainty. The charge misidentification rate in data varies from 0.2% at  $|\eta_{\text{det}}| = 0$  to 10% at  $|\eta_{\text{det}}| = 3.0$ , where tracking momentum resolution is poor. The statistical fluctuation in the measurement of the charge misidentification is used to estimate the final uncertainty on  $\sin^2 \theta_W$ .

## BACKGROUND

The background contamination is suppressed by the strict requirements on the matched track. The main contribution is from multijet events in which jets are mis-reconstructed as electrons, and is estimated from data. Multijet events are selected by reversing part of the electron selections to study the shape of the multijet background. This shape is considered to be different from the shape of the real multijet background which could pass all the electron selections. Therefore, a shape correction is developed by applying a scale factor between the efficiencies of EM-like jets (which are selected in a multijet-enriched data sample and could pass all the electron selections) and reversed selected jets as a function of  $p_T$ . The normalization of the multijet background is determined by fitting the sum of the invariant mass distributions from multijet and signal MC to the distribution from the selected data events. Other electroweak backgrounds are estimated using a PYTHIA MC simulation and found to be negligible around the  $Z$  pole. The total number of background events is found to be less than 1% in CC-CC events and less than 4% in CC-EC and EC-EC events.

## RESULTS

Comparisons of data to the sum of signal MC and background for the  $M_{ee}$  and  $\cos \theta^*$  distributions have been checked, and reasonable agreement is observed. The background-subtracted raw  $A_{FB}$  distributions are shown in Fig. 1 for CC-CC, CC-EC and EC-EC events. In the mass region around the  $Z$  pole, the variations of  $A_{FB}$  values for CC-EC events are much more pronounced than those in CC-CC and EC-EC ones, and thus CC-EC events are more sensitive to the weak mixing angle.

The weak mixing angle is extracted from the measured  $A_{FB}$  spectrum in the mass region of  $75 < M_{ee} < 115$  GeV/ $c^2$ , by comparing the data to the simulated  $A_{FB}$  templates corresponding to different input values of  $\sin^2 \theta_W$ . The MC templates are obtained by reweighting  $M_Z$  and  $\cos \theta^*$  distributions at the generator level into

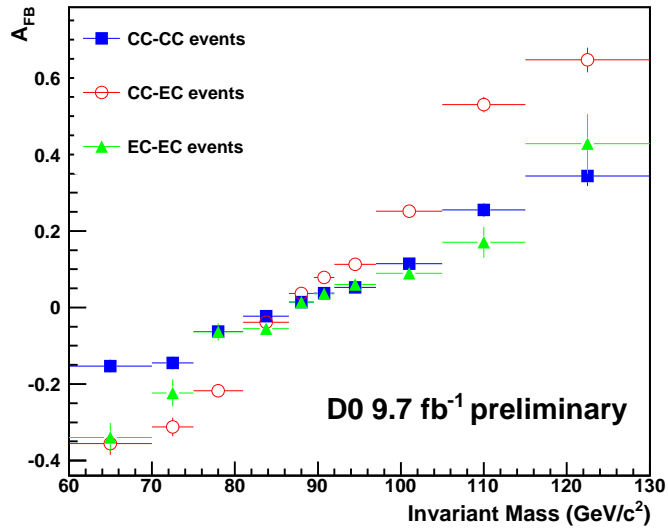


Figure 1: (color online). Background subtracted raw  $A_{FB}$  distributions measured in data.

	$\sin^2 \theta_W$	statistical uncertainty
CC-CC events	0.23086	0.00116
CC-EC events	0.23108	0.00047
EC-EC events	0.22910	0.00276
combined	0.23098	0.00042

Table 1: Measured  $\sin^2 \theta_W$  value and corresponding statistical uncertainties.

$\sin^2 \theta_W$	<b>0.23098</b>
statistical unc.	0.00042
Energy scale	0.00012
Energy smear	0.000018
Background	0.000008
Charge misID	0.000030
Electron ID	0.000066
Total systematic unc.	0.00014
total unc.	0.00044

Table 2: Measured  $\sin^2 \theta_W$  value and corresponding uncertainties but not including that due to PDF uncertainties. All uncertainties are symmetric. Higher-order theoretical corrections are not included.

different Born-level  $\sin^2 \theta_W$  predictions. The best  $\chi^2$ -fitting results of different event categories, and the statistical uncertainties of the measured  $\sin^2 \theta_W$ , are listed in Table 1.

The systematic uncertainties come from the energy modeling, electron identification, charge misidentification and background estimation. The systematic uncertainties are small compared to the statistical uncertainty. The uncertainties from electron identification and charge misidentification are estimated using the statistical uncertainties of the measured efficiencies and charge misidentification probability. The uncertainties of energy modeling are discussed before. The uncertainty from background estimation is dominated by the QCD normalization factor. The statistical uncertainty of the fitted factor is used in the final estimation. The uncertainties of  $\sin^2 \theta_W$  are still dominated by data statistics.

Due to the fact that all the systematic and statistical uncertainties in different categories are uncorrelated, the results can be combined by using the corresponding uncertainties as weights, giving  $0.23098 \pm 0.00042$  (stat.)  $\pm 0.00012$  (syst.)  $\pm 0.00029$  (PDF). The combined systematic uncertainties are listed in Tab. 2. The PDF uncertainty is estimated by using 40 CTEQ6.1M error sets which correspond to a 90% C.L. This is scaled to a 68% (one standard deviation) C.L. by applying a factor of 1/1.645.

In order to have a consistent SM definition and provide a result comparable with previous measurements, the PYTHIA interpretation of the weak mixing angle has been compared to RESBOS predictions, which is modified as in the ZFITTER [17] definition to include higher order electroweak corrections into the enhanced Born approximation (EBA). A constant 0.00008 positive shift in the full EBA prediction from RESBOS relative to the LO prediction from PYTHIA is found, and the leptonic effective weak mixing angle measured using the D0  $9.7 \text{ fb}^{-1} Z/\gamma^* \rightarrow e^+e^-$  data is  $\sin^2 \theta_{\text{eff}}^\ell = 0.23106 \pm 0.00053$ . The comparison between our measurement and other experimental results is shown in Fig. 2. The measurements are from the LEP  $b$ -quark forward-backward asymmetry,  $A_{FB}^{0,b}$ , the SLD left-right asymmetry,  $A_{lr}$ (SLD), the LEP  $\tau$ -lepton polarisation measurement,  $A_l(P_\tau)$ , the SLD lepton asymmetry,  $A_{FB}^{0,\ell}$ , the CDF forward-backward asymmetry,  $A_{FB}^{c,c}$  and  $A_{FB}^{\mu,\mu}$  [1].

## CONCLUSION

In conclusion, we have measured the effective weak mixing angle  $\sin^2 \theta_{\text{eff}}^\ell$  from the forward-backward charge asymmetry  $A_{FB}$  distribution in the process  $p\bar{p} \rightarrow Z/\gamma^* \rightarrow e^+e^-$  at the Tevatron. The data statistics are significantly enlarged by including electrons reconstructed in central calorimeter phi-mod module boundaries, electrons reconstructed in the high  $\eta_{\text{det}}$  region and EC-EC events. The primary systematic uncertainty is reduced by introducing a new electron energy calibration method, which unifies the position of the  $Z$  boson mass peak with a deviation smaller than 100 MeV in the data and 10 MeV in the MC. The final result from  $9.7 \text{ fb}^{-1}$  of D0 RunII data,  $\sin^2 \theta_{\text{eff}}^\ell = 0.23106 \pm 0.00053$ , is the most precise measurement from light quark interactions, and comparable to the world's best measurements performed by the LEP and SLD Collaborations. The measured value of  $\sin^2 \theta_{\text{eff}}^\ell$  is consistent with the average of LEP and SLD.

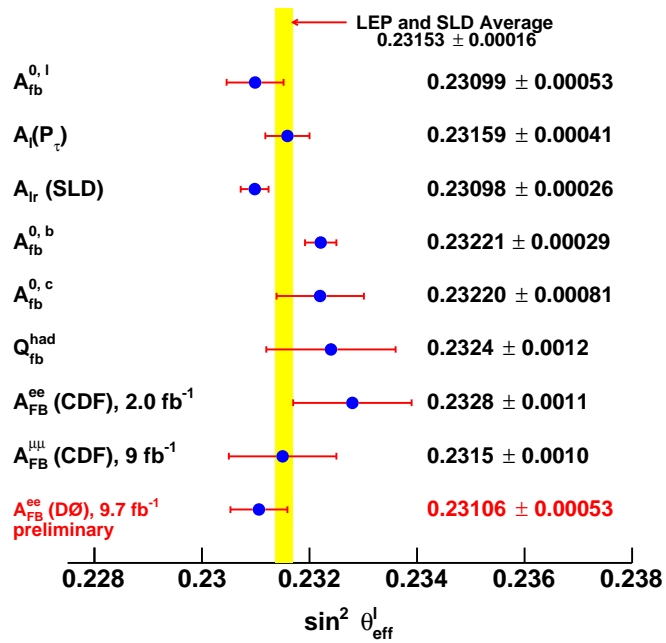


Figure 2: (color online). Comparison of measured  $\sin^2 \theta_{\text{eff}}^\ell$  with results from other experiments. The average is a combination of  $A_{FB}^{0,\ell}$ ,  $A_l(P_\tau)$ ,  $A_{lr}(SLD)$ ,  $A_{FB}^{0,b}$ ,  $A_{FB}^{0,c}$ , and  $Q_{FB}^{had}$  measurements from the LEP and SLD Collaborations [1].

# References

- [1] The ALEPH, DELPHI, L3, OPAL, SLD Collaborations, the LEP Electroweak Working Group, the SLD Electroweak and Heavy Flavour Groups, Phys. Rept. **427**, 257 (2006)
- [2] J. C. Collins and D.E. Soper, Phys. Rev. D **16**, 2219 (1977).
- [3] D. Acosta *et al.* (CDF Collaboration), Phys. Rev. D **71**, 052002 (2005).
- [4] T. Aaltonen *et al.* (CDF Collaboration), Phys. Rev. D **88**, 072002 (2013).
- [5] CDF Collaboration, CDF/PUB/ELECTROWEAK/PUBLIC/11056, arXiv:1402.2239.
- [6] V. M. Abazov *et al.* (D0 Collaboration), Phys. Rev. Lett. **101**, 191801 (2008).
- [7] V. M. Abazov *et al.*, (D0 Collaboration), Phys. Rev. D **84**, 012007 (2011).
- [8] S. Chatrchyan *et al.*, (CMS Collaboration), Phys. Rev. D **84**, 112002 (2011).
- [9] V. M. Abazov *et al.* (D0 Collaboration), Nucl. Instrum. Methods Phys. Res. A **565**, 463 (2006).
- [10] D0 uses a cylindrical coordinate system with the  $z$  axis along the beam axis in the proton direction. Angles  $\theta$  and  $\phi$  are the polar and azimuthal angles, respectively. Pseudorapidity is defined as  $\eta = -\ln[\tan(\theta/2)]$  where  $\theta$  is measured with respect to the interaction vertex. In the massless limit,  $\eta$  is equivalent to the rapidity  $y = (1/2)\ln[(E + p_z)/(E - p_z)]$ , and  $\eta_{\text{det}}$  is the pseudorapidity measured with respect to the center of the detector.
- [11] V. M. Abazov *et al.* (D0 Collaboration), arXiv:1401.0029 [hep-ex], accepted by Nucl. Instrum. Methods. Phys. Res. A.
- [12] T. Sjostrand *et al.*, Comp. Phys. Commun. **135**, 238 (2001). PYTHIA version v6.323 is used throughout.
- [13] J. Pumplin *et al.*, J. High Energy Phys. **07**, 012 (2002); D. Stump *et al.*, J. High Energy Phys. **10**, 046 (2003).
- [14] R. Brun and F. Carminati, CERN Program Library Long Writeup W5013, 1993 (unpublished).
- [15] V. M. Abazov *et al.* (D0 Collaboration), Phys. Rev. D **76**, 012003 (2007).
- [16] C. Balazs and C. P. Yuan, Phys. Rev. D **56**, 5558 (1997).
- [17] D. Y. Bardin *et al.*, Z. Phys. C **44** 493 (1989); D. Y. Bardin *et al.*, Comput. Phys. Commun. **59**, 303 (1990).